Journal of Power Sources 192 (2009) 57–62

Contents lists available at ScienceDirect

Journal of Power Sources

journal homepage: www.elsevier.com/locate/jpowsour

High surface area graphite as alternative support for proton exchange membrane fuel cell catalysts

P. Ferreira-Aparicio[a,*], M.A. Folgado[a], L. Daza[a,b]

[a] Centro de Investigaciones Energéticas, Medioambientales y Tecnológicas (CIEMAT), Avda. Complutense 22, E-28040 Madrid, Spain
[b] Instituto de Catálisis y Petroleoquímica (CSIC), C/Marie Curie, 2 Campus de Cantoblanco, E-28049 Madrid, Spain

ARTICLE INFO

Article history:
Received 9 October 2008
Received in revised form 17 November 2008
Accepted 2 December 2008
Available online 7 December 2008

Keywords:
High surface area graphite
PEMFC catalyst
Pt/HSAG
Temperature programmed oxidation
Interlamellar Pt

ABSTRACT

The suitability of a high surface area graphite (HSAG) as proton exchange membrane fuel cell (PEMFC) catalyst support has been evaluated and compared with that of the most popular carbon black: the Vulcan XC72. It has been observed that Pt is arranged on the graphite surface resulting in different structures which depend on the catalysts synthesis conditions. The influence that the metal particle size and the metal-support interaction exert on the catalysts degradation rate is analyzed. Temperature programmed oxidation (TPO) under oxygen containing streams has been shown to be a useful method to assess the resistance of PEMFC catalysts to carbon corrosion. The synthesized Pt/HSAG catalysts have been evaluated in single cell tests in the cathode catalytic layer. The obtained results show that HSAG can be a promising alternative to the traditionally used Vulcan XC72 carbon black when suitable catalysts synthesis conditions are used.

1. Introduction

Cost and durability are two major issues in proton exchange membrane fuel cell (PEMFC), which are intimately related. Costs reduction strategies usually consider decreasing the amounts of the most expensive elements or substituting some components by cheaper or more durable materials. Particularly, PEMFC electrodes constitute a large amount of the cost of the module, contributing to more than 40% on its whole expense [1]. One of the milestones for this technology consists in looking for alternative materials to enlarge PEMFC catalysts lifetime.

Carbon supports for PEMFC catalysts must combine a number of properties such as electron conductivity, corrosion resistance, surface properties, and low cost [2]. High surface area supports with high stability against corrosion, and providing strong interaction with the metal are good candidates for the synthesis of stable small nanoparticles with high metal specific surface areas [3,4]. A good combination of these characteristics could contribute to improve catalysts lifetime and performance. Several carbonaceous materials with different structures and specific surface areas have been tested. Some of them have yielded acceptable results, but no substitute for the Vulcan XC72 carbon black has been found yet and it still remains as the most extendedly used support for this application [5]. The extent of the carbon support graphitization has been found to play an important role on the catalyst stability, with more graphitic carbons being more thermally and electrochemically stable [2,6–10]. This improved stability has been attributed to the lower amount of defect sites on the carbon structure where carbon oxidation initiates [11].

Carbon corrosion itself is not the only mechanism contributing to PEMFC catalysts degradation. The properties of the metal crystallites on it, their interaction with the support, and the operation conditions also influence catalysts lifetime. Phenomena such as the so-called "Ostwald rippening", which is due to Pt dissolution and re-deposition in two and three dimensions, and/or the coalescence of particles, also contribute to the degradation process by decreasing the electrocatalytic surface area (ESA). Furthermore, working variables such as humidity, temperature, potential variation and cycling, or start-stop procedures, among others, may exacerbate degradation processes and reduce catalysts lifetime in membrane-electrode assemblies. The investigation on the durability of catalysts for application in PEMFCs is a complex and time-consuming task depending on numerous factors [12]. Analyzing their durability in a real normally working PEMFC requires tests lasting for several thousand hours [13,14]. In addition, finding out the origin of the performance loss is not always easy. Therefore, different accelerated degradation tests have been developed for PEMFC materials evaluation [6,15–17]. Methods such as thermal degradation under hot air conditions [6,18–19], aging in hot aqueous acid solution [7,14], open-circuit cell operation [20] or electrochemically forced aging under simulated cell conditions

* Corresponding author. Tel.: +34 913460897; fax: +34 913466269.
E-mail address: paloma.ferreira@ciemat.es (P. Ferreira-Aparicio).

0378-7753/$ – see front matter © 2008 Elsevier B.V. All rights reserved.
doi:10.1016/j.jpowsour.2008.12.003

[11,17,21–22] have been commonly used to analyze the PEMFC catalysts carbon corrosion [2].

In this paper, the suitability of a high surface area graphite (HSAG) as PEMFC catalyst support is evaluated and compared with that of the most popular carbon black, the Vulcan XC72. A temperature programmed oxidation (TPO) test under oxygen containing streams is proposed as a useful method to assess the resistance of PEMFC catalysts to carbon corrosion. The influence that the metal particle size and the metal-support interaction exert on the catalysts degradation rate and on a cathode performance in a single cell test is analyzed.

2. Experimental

2.1. Catalysts synthesis

Supported Pt catalysts have been prepared by applying a precipitation-reduction procedure. Two carbon supports have been used for the study: Vulcan XC72 from Cabot Corp., and TIMREX® high surface area graphite (HSAG 300) from Timcal, Ltd. The specific surface area of the supports has been estimated from N_2 adsorption isotherms at 77 K yielding values of 222 and 277 $m^2\,g^{-1}$, respectively.

For the synthesis, the required amount of the support was suspended in distilled water, heated up to 363 K, and agitated until obtaining a homogeneous dispersion. Then, an aqueous solution of H_2PtCl_6 was added under continuous stirring to obtain 15 wt.% Pt loading in the final catalyst. After adjusting the pH in the solution to basic values (>9.0) using $NaHCO_3$, a formaldehyde solution (37 vol.%) was added to the ink as reducing agent with a mol ratio $HCHO:PtCl_6^{2-} = 20:1$. The resulting mixture was reacted at 363 K for a 5 min period in the case of catalysts denoted with A, and for 15 min in catalysts denoted with B. Finally, the resulting solids were filtrated and washed with copious amounts of distilled water and dried overnight at 343 K.

2.2. Catalysts characterization tests

The exact metal loading in each catalyst has been gravimetrically determined by oxidizing the support. TPO tests have been carried in a thermobalance Mettler Toledo (TGA/SDTA851e). Aliquots of the catalysts have been placed in an alumina basket (70 μl) under a flow of N_2/O_2 and heated up to 1223 K at a rate of 25 K min^{-1}.

Powder X-ray diffraction analysis has been carried out on the fresh catalysts in order to evaluate the average particle size of the Pt aggregates formed on them. Diffractograms were recorded in a Panalytical X'Pert PRO diffractometer in a 4–90° 2θ range in a continuous scan mode with Cu Kα radiation (λ = 1.540598 Å). A volume average diameter has been estimated from the broadening of the Pt diffraction line corresponding to the (2 2 0) plane (2θ = 65.7).

Transmission electron microscopy (TEM) analysis has been also carried out in some of the catalysts to obtain direct images of individual Pt particles representative of the sample structure. A JEOL JEM 2100F microscope operating at 200 kV with a resolution of 0.19 nm was used. Powdered samples were ultrasonicated in alcohol for 5 min and then deposited on copper grids.

H_2 chemisorption measurements have been performed in a conventional glass volumetric apparatus equipped with a turbo pumping system (Varian Turbo V70 LP and SH110). Samples of 30 mg were charged in a glass bulb connected to the volumetric adsorption system and the air inside was evacuated. The pretreatment consisted in heating the sample at 473 K under dynamic vacuum and maintaining those conditions for 1 h [23]. The adsorption isotherm was measured after cooling the sample at 298 K. The chemisorbed amount has been calculated by extrapolating the linear part of the isotherm curve to zero equilibrium pressure.

2.3. Single cell catalyst evaluation tests

The synthesized Pt/C samples have been tested in single cells. A standard commercial gas diffusion electrode LT 120E-W/alt/StdN (PEMEAS, E-TEK, Inc.) containing 0.25 $mg_{Pt}\,cm^{-2}$ was used as anode. The Pt/C catalysts under study have been used as cathodic catalysts. Catalytic inks for cathodes were prepared by dispersing the catalyst in isopropylic alcohol with 30 wt.% of Nafion perfluorinated ion-exchange resin. The ink was then sprayed on the surface of an ELAT LT1200-W gas diffusion media from PEMEAS (E-TEK Inc.) using an automatized system. Although Pt loadings use to be higher in cathodes than in anodes, amounts as low as 0.1 $mg_{Pt}\,cm^{-2}$ have been used for the cathodes in this study. This unusually low Pt loading allows a comparative evaluation of the three synthesized catalysts by ensuring that the cathodes are limiting the cell performance. Membrane-electrode assemblies with an active electrode area of 15.2 cm^2 were mounted in the cell using a previously activated Nafion 117 polymer film. The cells were tested in a home-made system which allows real-time data acquisition (cell temperature, anode and cathode pressure, mass flow rates for gas feeding, voltage, current, etc.) and control of test parameters. After purging piping and anode and cathode gas compartments with humidified N_2, the cell was started-up with H_2 and O_2 streams

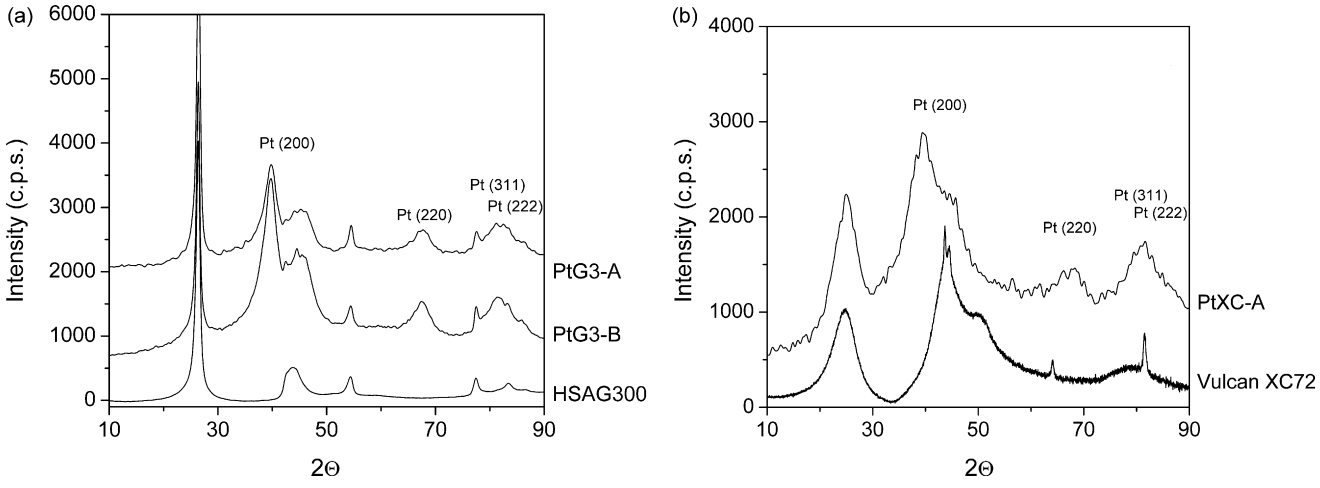

Fig. 1. X-ray diffractograms for the synthesized catalysts and their supports: (a) HSAG 300 (G3), PtG3-A and PtG3-B, and (b) Vulcan XC72 (XC) and PtXC-A.

and with a constant current demand for at least 12 h. Cell testing was carried out at 353 K, at different backpressures with fully humidified H_2 and O_2 streams, which were fed at constant stoichiometry ($\lambda_{H_2} = 1.5$, $\lambda_{O_2} = 3$). Polarization curves were obtained under those conditions. After single cell tests, the electrochemically active area of the cathode was determined in situ by cyclic voltammetry at several sweep-potential rates and at temperatures of 303 and 353 K.

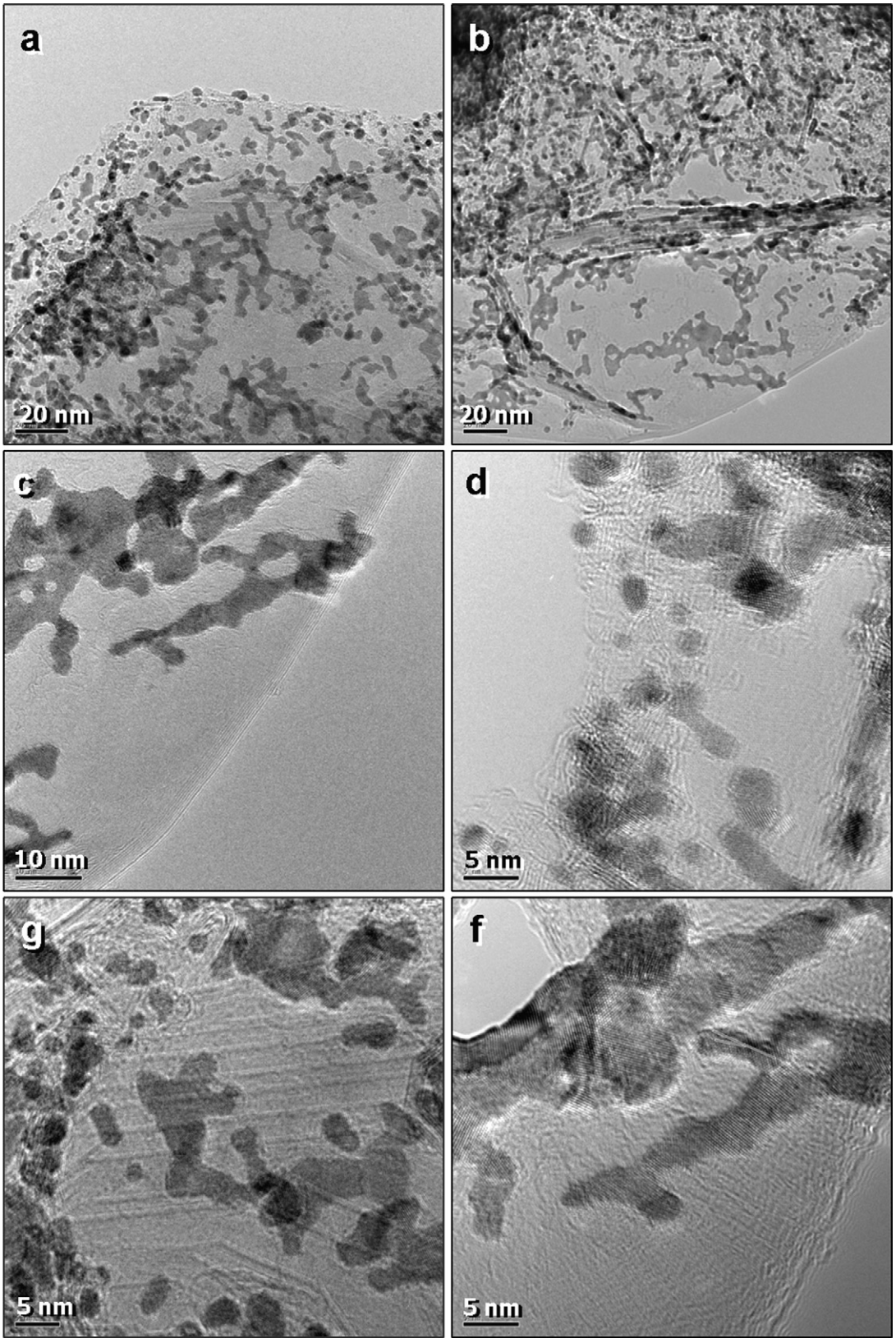

Fig. 2. (a–f) TEM micrographs showing the different Pt structures formed in PtG3-B.

Table 1
Physico-chemical properties of the synthesized catalysts.

Catalyst	Pt loading (wt.%)	d_{XRD} (nm)	S_{XRD} ($m^2\ g_{Pt}^{-1}$)	$(H/Pt)_{chem}$	S_{chem} ($m^2\ g_{Pt}^{-1}$)
PtG3-A	15.3	2.5 ± 0.5	97 ± 17	0.33	83 ± 8
PtG3-B	15.0	3.3 ± 0.2	84 ± 5	0.95	234 ± 23
PtXC-A	14.1	2.4 ± 0.5	116 ± 25	0.33	82 ± 8

3. Results and discussion

3.1. Structural characterization

Two Pt catalysts were synthesized on HSAG 300 by applying 5 and 15 min reduction periods. They have been denoted as PtG3-A and PtG3-B, respectively. A third catalyst supported on Vulcan XC72 was synthesized using a 5 min reduction period (PtXC-A), as a reference for comparison.

Fig. 1 shows comparatively the resulting X-ray diffractograms on catalysts and supports. The average volume diameter for Pt particles (d_{XRD}) and the Pt surface area (S_{XRD}) have been estimated from the broadening of the Pt diffraction line corresponding to the (2 2 0) plane ($2\theta = 65.7$). The obtained values are compiled in Table 1 together with those data obtained from H_2 chemisorption measurements (d_{Chem} and S_{Chem}). For the calculations, it is assumed that Pt particles have a spherical geometry and that their surface is formed by equal proportions of the main low index planes [24]. The estimations obtained from XRD and chemisorption measurements are in good agreement in the case of the catalysts prepared with a short reduction period of 5 min. However, there is a striking difference between them in the case of the PtG3-B catalyst, for which the reduction stage was extended for 15 min. TEM micrographs obtained for this sample unveil the origin of these discrepancies. Fig. 2 shows several images of the general structure of this catalyst at nanometric level (images a and b) and some details of the metal aggregates and particles formed (c–f). Two types of Pt structures are observed on the graphite platelets. The first one corresponds to very small spherical particles with diameters in the 2–3 nm range. The second type is associated to relatively large bidimensional aggregates. X-ray microanalysis (XMA) results confirmed the dark regions to be Pt metal. Although some of the Pt structures have sizes from 2 to 5 nm, most of them are much larger and, in some cases, may span at least in one direction even above 100 nm. A careful inspection of the images reveals that these structures are ordered following the orientation of the graphite platelets. The detailed observation of a number of sheets in parallel, as it can be observed in the central region of the image 'b' in Fig. 2, presumably indicates that platinum sheets exist between graphite layers and their growth takes place mainly in 2D. The increase of the synthesis time seems to favor the intercalation of the platinum between graphite interlayers. After reduction, bidimensional structures of Pt metal form aggregates like interlayered nanosheets with 2–3 nm thickness. According to several studies reviewed by Bezerra et al., Pt may undergo reconstruction after being reduced causing a surface redistribution of the adsorbed Pt towards the π sites in the basal planes of the graphitic crystallites [4]. This explains why in the case of the PtG3-B catalyst, in which there is a longer synthesis period, the XRD analysis provides evidence of formation of larger Pt structures, whereas the H/Pt ratio obtained by chemisorption indicates that most of the Pt atoms in the specimen are accessible for hydrogen adsorption. Shirai et al. observed the formation of similar platinum nanosheets of similar thickness between graphite layers using low surface area graphite (KS6 from Lonza) [25]. The formation of metal–graphite intercalation compounds has been intensively investigated in the last decades [26–34] because of their interesting catalytic and electrical properties.

3.2. Temperature programmed oxidation tests

In order to evaluate the chemical stability of the synthesized catalysts against corrosion of the support, TPO tests have been performed. The structural differences among the catalysts are also reflected in their analysis by TPO. The differential thermogravimetric curves for the catalysts and their supports during TPO are shown in Fig. 3. It can be observed that the particle size and the structure of the carbon influence the oxidation rate of the support. More ordered structures in carbon provide more stability against oxidation. Thus, the HSAG 300 support reaches its oxidation maximum 100° above Vulcan XC72, which has its maximum oxidation rate at 995 K (Fig. 3b).

The presence of Pt on the carbon materials catalyzes their oxidation. The Pt particle size has a large influence on the oxidation temperature of the support in the catalyst and it can be clearly appreciated in Fig. 3a. The larger structures in PtG3-B result in a maximum for the graphite oxidation rate (808 K), which takes place 100° above than in PtG3-A (708 K). A common characteristic in them is that both show a wide temperature range for oxidation resulting in broad peaks in the differential thermogravimetric curve. In the case of the PtXC-A specimen, the carbon black is combusted in a very thin temperature range. The combustion temperature of the Vulcan XC72 is reduced by 300° in the presence of Pt in PtXC-A, due to a fine particle distribution originating a very sharp peak in the differential thermogram.

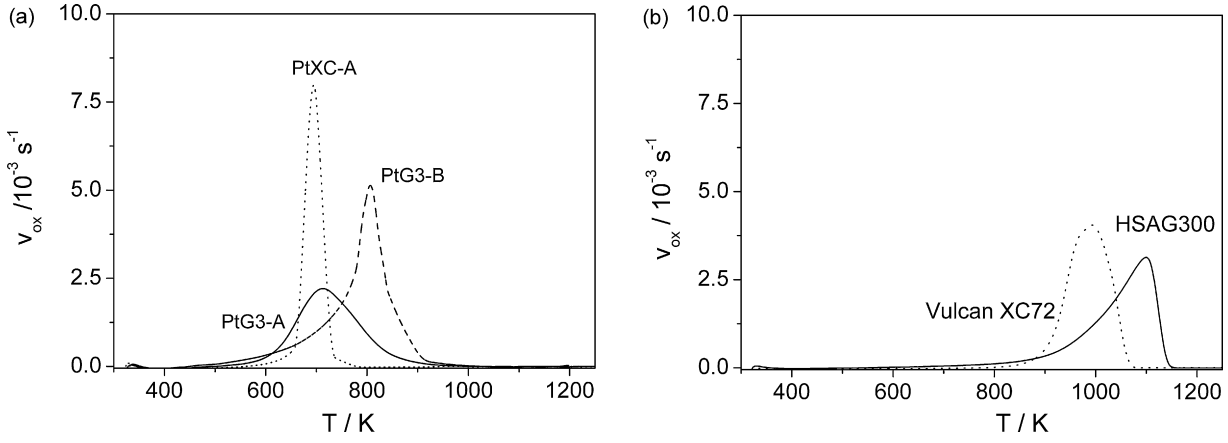

Fig. 3. Differential thermogravimetric curves in N_2/O_2 atmosphere: (a) HSAG supported catalysis (PtG3-A and PtG3-B) and Vulcan XC72 supported platinum (PtXC-A) and (b) carbon supports (HSAG 300 and Vulcan XC72).

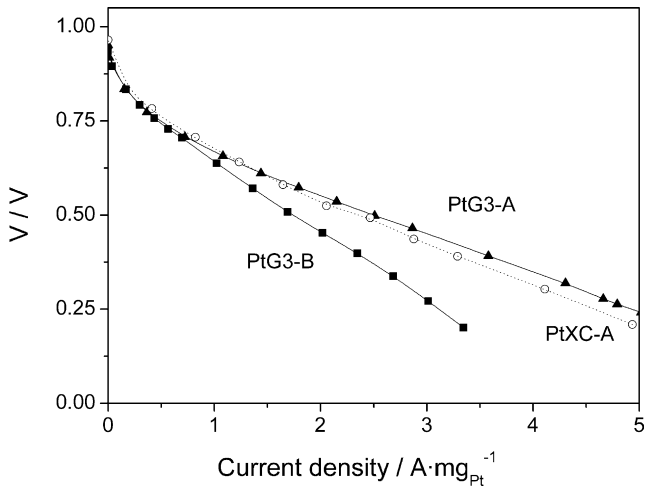

Fig. 4. Polarization curves obtained for single cells containing cathodes prepared with the synthesized catalysts: (▲) PtG3-A, (■) PtG3-B and (◯) PtXC-A.

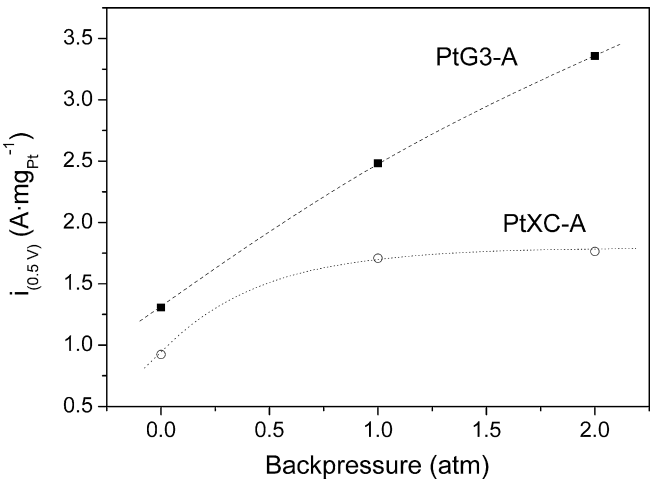

Fig. 5. Backpressure effect on single cell performance for MEAs with PtG3-A and PtXC-A as cathodic catalysts.

The differential thermogravimetric curves for the TPO of catalysts provides a useful tool for the assessment of one of the typical degradation mechanisms for cathodic layers in PEMFC electrodes. This process is not easy to evaluate in situ during cells testing, since it depends on numerous working variables and would take very long testing periods. Thus, a test such as TPO allows a relative comparison of stability against corrosion among the catalysts: PtG3-B > PtG3-A ≥ PtXC-A.

3.3. Single cell tests: electrochemical performance

The synthesized catalysts have been used to prepare gas diffusion electrodes (GDEs) with similar Pt loadings. These GDEs have been working as cathodes in single cells. Although the Pt loading in them is unusually much lower than that in the standard electrode working as anode, this configuration allows evaluating the synthesized catalysts comparatively ensuring that they limit the cell performance. The obtained polarization curves from the prepared membrane-electrode assemblies (MEAs) are presented comparatively in Fig. 4. The cell containing PtG3-A in the cathode catalytic layer exhibits a good behavior at high current densities as compared to PtXC-A, and especially to PtG3-B. Table 2 summarizes the Pt loading in each cathode, the Pt specific activity in each MEA at 0.9 V and at 1 atm backpressure, and the electrochemical area of the cathode after cell testing. The specific activity obtained at 0.9 V for PtXC-A is very similar to that reported by Gasteiger et al. as benchmark for the commercial Pt(20 wt.%)/Vulcan XC72 from E-TEK under analogous conditions [14]. The specific activities obtained for both PtG3 specimens at 0.9 V are similar, and lower than that obtained for the Vulcan XC72-supported sample.

On the other hand, the electrochemical surface areas (ECSA) obtained by in situ CV at 303 K for the cathodes with graphite catalysts differ considerably. The ECSA value obtained for PtG3-A threefolds that obtained in the MEA with the PtG3-B catalyst, indicating a better Pt utilization in PtG3-A. A large proportion of the Pt surface accessible for H_2 in the PtG3-B catalyst during chemisorption measurements seems to be electrochemically inactive in the cathode. The ECSA values for cathodes resemble the better behavior shown by PtG3-A at large current densities as compared to that of PtG3-B.

It must be considered that the evaluation of the samples as cathodic catalysts in a cell can be influenced by other parameters affecting the MEA performance such as the electrode permeability or the gas accessibility to the active sites. The structural characteristics of the graphite supported samples, in particular that of the PtG3-B sample, probably difficult the accessibility of oxygen to the electrochemically active sites.

PtG3-A and PtXC-A cathodes contain catalysts with similar average Pt particle sizes and metal surface area (Table 1). Thus, the influence that the support structure exerts on the cells performance can be better analyzed in them. Fig. 5 shows the effect of the backpressure increase on the current density obtained at 0.5 V. For the cell with the PtXC-A cathode catalyst, the backpressure increase above 1 atm does not yield any significant performance improvement, whereas there is a practically linear proportionality among both parameters in the case of the cell with the PtG3-A catalyst. This effect can be attributed to the different oxygen accessibility to the cathode catalytic layer. Both electrodes are prepared on the same GDM, which consists of a hydrophobized carbon cloth with a carbon black/PTFE layer. In this substrate, oxygen diffuses from the flow field to the active layer according to Fick's law. At low pressure the diffusion mechanism is mixed Knudsen and molecular diffusion [35,36]. As shown in Fig. 5 for PtXC-A, the limiting current increases with pressure via a Knudsen mechanism in the low backpressure range, and then it becomes constant as molecular diffusion takes over [36]. In the case of the PtG3-A cathode catalyst, the oxygen mass transfer resistance is larger and increasing the backpressure up to 3 atm results in better cell performance.

Regarding the size of the Pt aggregates and their distribution on the graphite support, it has been shown that small Pt particles in the outer surface of HSAG 300 platelets, as in the case of the PtG3-A specimen, yield a good performance, which is comparable to that achieved with analogous Vulcan XC72 supported catalysts, and much better than that obtained with Pt on HSAG 300 when interlamellar bidimensional structures are formed (PtG3-B). Although

Table 2
Properties of the membrane-electrode assemblies prepared with the synthesized catalysts in the cathode and E-TEK commercial GDE in the anode (0.25 mg_{Pt} cm^{-2}).

Catalyst	Cathode loading (mg_{Pt} cm^{-2})	$I_{m\,(0.90\,V)}$ (A mg_{Pt}^{-1})	$(H/Pt)_{chem}$	$A_{MEA,\,cathode}$ (EPSA) (m^2 g_{Pt}^{-1})
PtG3-A	0.09	0.045	0.33	20
PtG3-B	0.07	0.045	0.95	6
PtXC-A	0.11	0.097	0.33	n.d.

the Pt surface area for this latter catalyst is very high as measured by H_2 chemisorption, the Pt utilization as determined by CV is very low. The formation of the triple phase boundary in this sample probably requires the polymer added in the catalytic ink to be infiltrated in the graphite structure to be in contact with Pt aggregates. This is a plausible explanation for the low Pt utilization measured by CV in that sample with very high Pt dispersion.

3.4. Conclusions

A HSAG has been evaluated as catalyst support for PEMFC. The results show that it can be a good alternative to the popular Vulcan XC72 with higher resistance against corrosion. Two Pt catalysts have been synthesized on HSAG by means of a precipitation–reduction method. The structure and distribution of the Pt particles on the HSAG surface has been observed to change by extending the synthesis stage. Whereas small particles are distributed on the outer HSAG surface for short synthesis periods, by extending their duration, the formation of extended bidimensional aggregates is favored. The formation of the 2D structures, as shown by TEM imaging, seems to be due to the intercalation of the metal between graphite platelets. In the specimen with longer synthesis period, in which bidimensional structures are predominant, large discrepancies have been found in particle size estimations using two techniques such as H_2 chemisorption and the broadening of the Pt X-ray diffraction lines. These differences can be mainly attributed to the formation of those bidimensional aggregates.

TPO tests of the synthesized catalysts reveal that catalysts supported on HSAG are more stable against corrosion than Vulcan XC72 supported samples. The stability of the samples is clearly illustrated by differential thermogravimetric curves during their temperature-programmed oxidation. The oxidation temperature of the carbon support in each catalyst is shown to be closely related to the size of the aggregates and the extent of the perimeter between both phases.

Pt utilization, as determined in situ by cyclic voltammetry in a membrane-electrode assembly, has been observed to be very low in cathodes containing HSAG catalysts in which interlamellar Pt prevails. This indicates that most of the metal surface in such structure is not electrochemically active. On the other hand, when Pt is mainly on the outer HSAG surface in the form of small crystallites with diameters in the 2–3 nm range, the cathodes show even better performance than similar catalysts supported on Vulcan XC72.

Acknowledgments

The authors thank the Spanish Ministry for Education and Science and the Comunidad de Madrid for financial support under Projects MEDEA (ENE2005-08799-C02-01/ALT) and ENERCAM-CM (S-0505/ENE-304), respectively.

References

[1] H. Tsuchiya, O. Kobayashi, Int. J. Hydrogen Energy 29 (2004) 985.
[2] Y. Shao, G. Yin, Y. Gao, J. Power Sources 171 (2007) 558.
[3] X. Yu, S. Ye, J. Power Sources 172 (2007) 133.
[4] C.W.B. Bezerra, L. Zhang, H. Liu, K. Lee, A.L.B. Marques, E.P. Marques, H. Wang, J. Zhang, J. Power Sources 173 (2007) 891.
[5] M. Kim, J.-N. Park, H. Kim, S. Song, W.-H. Lee, J. Power Sources 163 (2006) 93.
[6] D.A. Stevens, M.T. Hicks, G.M. Haugen, J.R. Dahn, J. Electrochem. Soc. 152 (2005) A2309.
[7] X. Wang, W. Li, Z. Chen, M. Waje, Y. Yan, J. Power Sources 158 (2006) 154.
[8] Y. Shao, Investigation on the stability of Pt/carbon nanotube catalysts and novel methods for the preparation of the electrodes for PEMFC, Ph.D. Thesis, Harbin Institute of Technology, Harbin, China, 2006.
[9] B.J. Eastwood, P.A. Christensen, R.D. Armstrong, N.R. Bates, J. Solid State Electrochem. 3 (1999) 179.
[10] F. Coloma, A. Sepúlveda-Escribano, F. Rodríguez-Reinoso, J. Catal. 154 (1995) 299.
[11] Y.Y. Shao, G.P. Yin, J. Zhang, Y.Z. Gao, Electrochim. Acta 51 (2006) 5853.
[12] J. Xie, D.L. Wood, D.M. Wayne, T.A. Zawodzinski, P. Atanassov, R.L. Borup, J. Electrochem. Soc. 152 (2005) A104.
[13] S.D. Knights, K.M. Colbow, J. St-Pierre, D.P. Wilkinson, J. Power Sources 127 (2004) 127.
[14] H.A. Gasteiger, S.S. Kocha, B. Sompalli, F.T. Wagner, Appl. Catal. B: Environ. 56 (2005) 9.
[15] P.J. Ferreira, G.J. La, O.Y. Shao-Horn, D. Morgan, R. Makharia, S. Kocha, H.A. Gasteiger, J. Electrochem. Soc. 152 (2005) A2256.
[16] M. Cai, M.S. Ruthkosky, B. Merzougui, S. Swathirajan, M.P. Balogh, S.H. Oh, J. Power Sources 160 (2006) 977.
[17] H.R. Colon-Mercado, H. Kim, B.N. Popov, Electrochem. Commun. 6 (2004) 795.
[18] D.A. Stevens, J.R. Dahn, Carbon 43 (2005) 179.
[19] O.A. Baturina, S.R. Aubuchon, K.J. Wynne, Chem. Mater. 18 (2006) 1498.
[20] Z.G. Qi, S. Buelte, J. Power Sources 161 (2006) 1126.
[21] Y.Y. Shao, G.P. Yin, Y.Z. Gao, P.F. Shi, J. Electrochem. Soc. 153 (2006) A1093.
[22] H.R. Colon-Mercado, B.N. Popov, J. Power Sources 155 (2006) 253.
[23] P. Ferreira-Aparicio, Chem. Mater. 19 (2007) 6030.
[24] J.R. Anderson, Structure of Metallic Catalysts, Academic Press, New York, 1975, pp. 295–297.
[25] M. Shirai, K. Igeta, M. Arai, Commun. Chem. (2000) 623.
[26] M.E. Vol'pin, Y.N. Novikov, Pure Appl. Chem. 60 (8) (1988) 1133.
[27] A. Mastalir, F. Notheisz, M. Bartok, Catal. Lett. 35 (1995) 119.
[28] L.B. Ebert, J. Mol. Catal. 15 (1982) 275.
[29] A. Fürstner, R. Csuk, C. Rohrer, H. Weidmann, J. Chem. Soc., Perkin Trans. I (1987) 1729.
[30] R. Csuk, B.I. Glanzer, A. Fürstner, Adv. Organomet. Chem. 28 (1988) 83.
[31] A. Fürstner, H. Weidmann, J. Organomet. Chem. 354 (1988) 15.
[32] G. Sirokmám, Á. Mastalir, Á. Molnár, M. Bartók, Z. Schay, L. Guczi, J. Catal. 117 (1989) 558.
[33] A. Fürstner, F. Hofer, H. Weidmann, J. Catal. 118 (1989) 502.
[34] G. Sirokmán, Á. Mastalir, Á. Molnár, M. Bartók, Z. Schay, L. Guczi, Carbon 28 (1990) 35.
[35] T.E. Springer, M.S. Wilson, S. Gottesfeld, J. Electrochem. Soc. 140 (1993) 3513.
[36] C. Boyer, S. Gamburzev, A.J. Appleby, J. Appl. Electrochem. 29 (1999) 1095.